Published in final edited form as:
*Biochemistry*. 2009 June 16; 48(23): 5057–5065. doi:10.1021/bi900337d.

# Snapshots of Dynamics in Synthesizing $N^6$-isopentenyladenosine at tRNA Anticodon,†,‡

**Sarin Chimnaronk**[1,4,*], **Farhad Forouhar**[2], **Junichi Sakai**[1], **Min Yao**[1], **Cecile M. Tron**[3], **Mohamed Atta**[3], **Marc Fontecave**[3], **John F. Hunt**[2], and **Isao Tanaka**[1,*]

[1]Faculty of Advanced Life Sciences, Hokkaido University, Kita-ku, Sapporo 060-0810, Japan [2]Department of Biological Sciences, Northeast Structural Genomics Consortium, Columbia University, New York, NY 10027, USA [3]IRTSV,CEA/CNRS/UJF, LCBM, UMR5249, 38054 Grenoble, France [4]Institute of Molecular Biology and Genetics, Mahidol University, Salaya Campus, Nakornpathom 73170, Thailand

## Abstract

Bacterial and eukaryotic transfer RNAs that decode codons starting with uridine have a hydrophobically-hypermodified adenosine at the position 37 ($A_{37}$) adjacent to the 3′-end of the anticodon, which is essential for efficient and highly accurate protein translation by the ribosome. However, it remains unclear how the corresponding tRNAs are selected to be modified by alkylation at the correct position of the adenosine base. We have determined a series of the crystal structures of bacterial tRNA isopentenyltransferase (MiaA) in apo- and tRNA-bound forms, which completely render snapshots of substrate selections during modification of RNA. A compact evolutionary inserted domain (herein ‘swinging domain’) in MiaA that exhibits as a highly mobile entity moves around the catalytic domain as likely to reach and trap the tRNA substrate. Thereby, MiaA clamps the anticodon stem loop of tRNA substrate between the catalytic and swinging domains, where the two conserved elongated residues from the swinging domain pinch the two flanking $A_{36}$ and $A_{38}$ together to squeeze out $A_{37}$ into the reaction tunnel. The site-specific isopentenylation of RNA is thus ensured by a characteristic pinch-and-flip mechanism and by a reaction tunnel to confine the substrate selection. Furthermore, combining information from soaking experiments with structural comparisons, we propose a mechanism for the ordered substrate-binding of MiaA.

†We are grateful to the staffs of beamlines BL41XU at SPring8 (Harima, Japan), and X4C at the National Synchrotron Light Source (NSLS) for their assistance during data collection. This research was supported in part by the National Project on Protein Structural and Functional Analyses from the Ministry of Education, Culture, Sports, Science, and Technology of Japan (MEXT) (to I.T.), and in part by a Human Frontier Science Program Research grant (to I.T.). S.C. was supported by a Grant-in-Aid for Young Scientists B from the Japan Society for the Promotion of Science (JSPS), and a grant for new researcher from the Thailand Research Fund (TRF). We thank Rong Xiao, Tom B. Acton and Gaetano T. Montelione, Mariam Abashidze, Helen Neely, and Jayaraman Seetharaman for cloning, expression, purification, crystallization, and data collection of the apo MiaAs from *B. halodurans* and *S. epidermidis*. The research on structural studies of apo MiaAs was supported by grants from the Protein Structure Initiative of the National Institutes of Health (P50 GM62413 and U54 GM074958).

‡Atomic coordinates and structure factors have been deposited in the Protein Data Bank (PDB) with accession codes 2ZM5 for *E. coli* MiaA–tRNA complex, 2ZXU for the ternary complex of *E. coli* MiaA–tRNA–DMASPP, 2QGN and 3EXA for the catalytic domain and the full-length *B. halodurans* (BH2366) MiaA, respectively, and 3D3Q for the full-length *S. epidermidis* (SE0981) MiaA.

*To whom correspondence should be addressed. S.C.: mbscr@mahidol.ac.th; Tel, +66 (0)2 800 3624 ext. 1468; Fax, +66 (0)2 441 9906. I.T.: tanaka@castor.sci.hokudai.ac.jp; Tel: +81 (0)11 706 3221; Fax: +81 (0)11 706 4905.

SUPPORTING INFORMATION AVAILABLE Supporting Information including detailed experimental procedures, eight figures, a crystallographic statistics table, and the supplemental references is available online via http://pubs.acs.org.

**Keywords**

tRNA; post transcriptional modification; crystal structure; translation; RNA chaperone

Nucleosides in the anticodon loop of tRNA are generally decorated by extensive post-transcriptional chemical modifications that contribute to efficiency and fidelity of protein synthesis on the ribosome (1-3). In bacterial and eukaryotic organisms, a subset of tRNA species that read the codons in mRNA starting with adenosine or uridine always contain a hypermodified nucleoside at the 3′-adjacent adenosine ($A_{37}$) to the anticodon (4). Such a bulky and hydrophobic hypermodification is thought to be involved in stabilizing the intrinsic weak A–U pairing interaction between anticodon and codon in the decoding, hypothesized by two rationales. First, the hydrophobic alkyl moiety may destabilize a closed conformation of the anticodon loop and imparts thermodynamic stability to the canonical $U_{33}$-turn conformation resulting in exposure of the Watson-Crick faces of the anticodon prior to decoding (5,6). Second, alkyl group likely improves interstrand base stacking interactions of the codon-anticodon minihelix in the A-site on the ribosome (7,8).

In *Escherichia coli*, $A_{37}$ in ten tRNAs that have $A_{36}$ as the third letter of the anticodon sequence (*i.e.*, read codon starting with U) are replaced by $N^6$-isopentenyladenosine ($i^6A$) or its hypermodified derivative 2-methylthio-$N^6$-isopentenyladenosine ($ms^2i^6A$), whereas thirteen tRNAs with $U_{36}$ anticodon possess $N^6$-threonylcarbamoyladenosine ($t^6A$) derivatives at the position 37 for efficient reading of codon with the first A letter (9,10). The enzyme tRNA isopentenyltransferase (MiaA) catalyzes addition of 5-carbon isopentenyl moiety to the exocyclic amine of $A_{37}$, utilizing dimethylallyl pyrophosphate (DMAPP) as the donor to produce $i^6A$ in tRNA (11-15). This initial step is absolutely required for the further methylthiolation of the $i^6A$ intermediate to $ms^2i^6A$ by MiaB (16,17) (Fig. S2B in the online supporting information). *E. coli* MiaA defective strain revealed multiple malfunctions in translational processes including codon context sensitivity, elongation rate, efficiency, and fidelity, leading to slow cellular growth and temperature sensitivity (18-23). Numerous lines of evidence also suggest that a wide range of cellular activities are affected by the presence of $i^6A$ including amino acid biosynthesis, aromatic amino acid uptake, and cellular response to environmental stress (24-27). Interestingly, *cis*-zeatin-type cytokinins, which display hormone-like functions as regulations of cell division and differentiation in plants, are produced by degradation of tRNA containing $i^6A$ (28). In mammals, MiaA homologues and their synthetic $i^6A$ are capable of suppressing tumor cell but likely through different pathways (29,30).

Extensive efforts utilizing either kinetics measurement or mutagenesis of both tRNA and protein have provided findings that MiaA predominantly recognizes a conserved consensus sequence $A_{36}A_{37}A_{38}$ in the anticodon loop of tRNA (Fig. S2A), and tRNA-binding precedes and is a prerequisite for efficient DMAPP-binding by the enzyme, thereby representing an ordered substrate binding mechanism (31-33). Recent crystallographic analyses of MiaA and its orthologue clarified that MiaA has plausibly evolved from a compact nucleotide kinase with a similar usage of the P-loop in binding pyrophosphate group (34,35). More importantly, MiaA harbors a reaction tunnel traversing through the center of the catalytic domain, to which the accepting tRNA and donating DMAPP substrates enter from opposite sides so as to meet at the middle of the tunnel (35). Very recently, a crystallographic structural analysis of an eukaryotic MiaA orthologue in complex with tRNA from budding yeast was reported when this manuscript was in process of preparation (36). Whereas the published results clearly revealed the architecture of the small ‘swinging’ domain of MiaA for the first time, and illustrated a mechanism for tRNA recognition, definite roles of the swinging domain in conformational rearrangement of tRNA and reaction catalyst remain mostly controversial.

Moreover, the structural information of dynamic of the swinging domain was so far unobserved. Here we present a series of crystal structures of bacterial MiaA orthologues in both apo-forms and in complex with tRNA in the absence or presence of a DMAPP analogue. Our combined results reveal a remarkable dynamic structural rearrangement of both protein and its substrate RNA in substrate selection and accommodation prior to catalysis, thereby completing animated motions of MiaA's action in modifying RNA.

## MATERIALS AND METHODS

### Preparation of Proteins and tRNAs

The *E.coli* MiaA gene (316 amino acids; 35 kDa) was expressed as a thrombin-protease-cleavable N-terminal hexahistidine tag fusion. Native and seleno-methionine (Se-Met) labeled protein were purified by Ni affinity and gel filtration chromatography, and the affinity tag removed by thrombin protease treatment at 4°C. The production of two full-length bacterial orthologues of MiaA, *Bacillus halodurans* BH2366 and *Staphylococcus epidermidis* SE0981, were carried out as part of the high-throughput protein production process of the Northeast Structural Genomics Consortium (NESG) (37). All recombinant MiaA orthologues were validated for their intact activities utilizing either the electrophoretic mobility shift assay (EMSA) or the *in vitro* isopentenyltransferase assay. *In vitro* runoff transcribed tRNAs were prepared as previously described (38). The oligo DNAs used to construct *E. coli* $tRNA^{Met}$ were as follows. 5′-primer: ***TAATACGACTCACTATA***GCCCGGATAGCTCAGTCGGTAG (forward); middle template: GGATAGCTCAGTCGGTAGAGCAGGGGATTGAAAATCCCCGTGTCCTTGGTTCGATTCCG (forward); 3′-primer: TGmGTGCCCGGACTCGGAATCGAACCAAGGAC (reverse); in which the T7 promotor sequence is in bold characters and complementary regions are underlined. Gm represents 2′-*O*-methyl deoxyguanosine, used for manipulating the uniform 3′-end of transcribed products (39).

### Crystallization

Purified *E. coli* MiaA and $tRNA^{Phe}_{GAA}$ were mixed in a molar ratio of 1.5:1, and the resulting mixture was incubated for 30 min at 25°C. The mixture was then injected into a Superose 12 size-exclusion column running at 4°C. Fractions containing MiaA–tRNA complex were collected and concentrated to 10-15 mg/ml by ultrafiltration (Ultra-4, Amicon) for immediate crystallization trial. Crystallization was basically carried out by using the hanging drop vapor diffusion method at 18-20°C. Protein samples were mixed with an equal volume of the reservoir solutions for initial crystallization trial. Initially, the *E. coli* MiaA–tRNA complex was obtained with a well solution containing 0.1 M MES pH 5.5-6.5, 15-24% PEG 8000, and 150-250 mM calcium acetate as a precipitant, and was further improved by addition of the Crystal Screen Kit I No. 40 comprising 0.1 M tri-sodium citrate dihydrate pH 5.6, 20% iso-propanol, and 20% PEG 4000 (Hampton Research) into the crystallization drop. Moreover, high-quality crystals of intact BH2366 were occasionally grown in the condition containing 16% PEG 3350 and 200 mM ammonium tartrate as precipitant in a few days, while full-length SE0981 was crystallized with a reservoir consisting of 100 mM MES (pH 6.15), 18% PEG 3350, and 100 mM KSCN. Crystals were harvested and transferred to the mother liquor plus 20% glycerol (for *E. coli* MiaA–tRNA complex) or 25% ethylene glycol (for BH2366 and SE0981) for cryoprotection and then flash-frozen in nitrogen cryostream or liquid propane, respectively.

### Structure determination and refinement

Each single-wavelength anomalous diffraction (SAD) dataset was collected under cryogenic condition (100 K) at the peak absorption wavelength of selenium, at the BL41XU stations of SPring8 (Harima, Japan) for *E. coli* complex, and on beamline X4C of the National Synchrotron Light Source (NSLS) for BH2366 and SE0981. These were indexed, integrated, scaled, and

merged using the HKL2000 package (40). For phase solution, the programs SHELX (41) or BnP (42) were used to locate most of selenium (Se) sites in the asymmetric unit of each crystal. These sites were used to initiate iterative phasing and automated model building in SOLVE/RESOLVE (43). In the case of *E. coli* MiaA–tRNA complex, model building was further achieved and refined with the program LAFIRE (44) running together with CNS (45). Completion of the structures was straightforward using iterative cycles of manual model building in Coot (46) or XtalView (47), and computational refinement in CNS. Additional details are provided in the Online Supporting Information. All molecular graphics were created using PyMol (48).

## RESULTS AND DISCUSSION

### MiaA clamps the anticodon helix of tRNA triggering backbone distortion

We have successfully purified and crystallized bacterial MiaA complexed with unmodified $tRNA^{Phe}_{GAA}$ from *E. coli* (see details in Materials and Methods, and Fig. S3 and Table S1 in Supporting Information). MiaA is a two-domain protein composed of the catalytic core and a compact α-helical domain (Figs. 1A and 1B). The overall structure of the catalytic domain of MiaA is nearly identical to the two previously reported MiaA structures from *Bacillus halodurans* (PDB ID: 2QGN with an rmsd of 1.13 Å for 214 pairs of Cα atoms compared) and *Pseudomonas aeruginosa* (225 Cαs' rmsd = 0.79 Å) (34), indicating that no substantial structural change is required for tRNA binding by the catalytic domain. The compact inserted 'swinging domain' (residues 127-186 in *E. coli* MiaA) is entirely visible revealing an antiparallel five-helical bundle with an alternating up-down topology. The swinging domain is connected to the catalytic domain by two extended loops (~8 amino acids) between α4 and β5. The fold of the swinging domain and its tRNA-binding manner are unique and not seen in other RNA-binding proteins.

MiaA exclusively binds to the anticodon helix of tRNA comprising nucleotides $A_{26}$-$C_{41}$ (Figs. 2A and 2B). The anticodon stem loop is tightly clamped between the catalytic domain and the swinging domain, burying 37% (1,058 $Å^2$) of the surface area of the anticodon helix in the interface. Drastic structural rearrangement of RNA backbones is observed at the bottom of the anticodon helix (Figs. 2A and 3A). The breakdown of base stacking of the anticodon triplet leads to the collapse of the canonical $U_{33}$-turn motif and splaying out of $U_{33}$-$G_{34}$-$A_{35}$ from the anticodon loop. Subsequently, the to-be-modified $A_{37}$ base flips out of the anticodon loop and buries itself into the reaction tunnel. The structural rearrangements of the anticodon loop are thus ascribed to two simultaneous steric interferences from both sides of the anticodon helix. On one hand, α14 of the catalytic domain invades the major groove of the anticodon helix, and broadens its width by 6.6 Å. On the other hand, two conserved elongated residues Gln166 and Arg167, residing at the tip of α8 in the swinging domain, synergize the conformational constraint by pinching the two $A_{37}$-flanking $A_{36}$ and $A_{38}$ together, which induces a sharp bent '<' shape of the anticodon loop with $A_{37}$ at the pointed tip. MiaA therefore acts like a press machine with the catalytic domain being the 'die' and the swinging domain the 'press'. The two flanking adenosines likely contribute further to correctly flipping the target $A_{37}$ into the tunnel by the pinching mechanism of Gln166 and Arg167 fingers. Whereas Gln166 is conservatively substituted by bulky charge residues, Arg167 is strictly conserved among species. Substitution of Arg167 by alanine resulted in substantial reduction in the catalytic efficiency, as $K_m$ increased 20-fold and nearly 10-fold for RNA and DMAPP, respectively, when compared with those of the wild type (32). The reduction in $K_m$ for DMAPP may be ascribed to a defective 'pinching finger' Arg167 that could not squeeze out $A_{37}$ into the tunnel to stack with the cofactor (see below). Interestingly, R176A mutant was tolerant of the A38G substitution in ASL, and even lowered $K_m$ by 2-fold for RNA. These results together with the

current structures clearly shed light onto the critical role of a 'pinch-and-flip' mechanism in tRNA discrimination, cofactor binding, and reaction catalysis by MiaA.

### MiaA indirect readout of the $A_{36}A_{37}A_{38}$ sequence

The exposed $A_{37}$ base is readily recognized by an invariant Asp42 at the end of β2, while it forms a hydrogen bond with the main chain of Thr54 (Figs. 2A, 2B). The $A_{37}$ purine ring is additionally sandwiched between two hydrophobic Leu45 and Val249 residues. Side chains of Ser43 and Thr108 donate hydrogen bonds to the phosphate group of $A_{37}$, while the next $A_{38}$ phosphate moiety is recognized by Arg281. The three residues that are involved in anchoring the phosphate groups flanking $A_{37}$ are all well conserved, which underscores the importance of stabilization of the RNA backbone in base flip-out. In contrast to the high specificity of the $A_{37}$ recognition, its neighboring $A_{36}$ and $A_{38}$ are less discriminated. While their purine bases are verified through the two 'pinching fingers' Gln166 and Arg167 of the swinging domain, adenine-specific N6 atom is not recognized by the enzyme. Intriguingly, discrimination of $A_{36}$ and $A_{38}$ is achieved through specific intramolecular interactions with the phosphate group of $U_{33}$, and the oxygen O2 atom of $U_{32}$, respectively (Figs. 2A and 2B). $U_{33}$ is universally conserved in the anticodon loop of tRNA, whereas $U_{32}$ can be replaced by pseudouridine (Ψ), cytidine, or 2′-*O*-methylcytidine in native *E. coli* tRNA substrates, all of which retain O2 atom at the same position for the hydrogen bonding. These, therefore, clearly elucidate the mechanism of MiaA indirect readout of the tRNA body for recognition of the consensus $A_{36}A_{37}A_{38}$ as an identity element.

### Direct recognition of the anticodon helix by MiaA

Interestingly, there is a tRNA embedding the identity $A_{36}A_{37}A_{38}$ sequence in the anticodon loop, which is not recognized by MiaA in *E. coli*. This isoacceptor $tRNA^{Ser}_{GGA}$, encoding UCY (Y = C or U) codon, contains $A_{37}$ that remains mysteriously unmodified (Fig. S2A). In our complex structure, in addition to the specific recognition of $A_{37}$, two other specific protein–RNA interactions are observed in the anticodon stem region (Fig. 2A). In particular, the base G29 at the middle of the anticodon stem forms a hydrogen-bond with the conserved Lys280 of the invading α14 helix. This position is substituted by a pyrimidine C in $tRNA^{Ser}_{GGA}$. The critical role of direct discrimination by Lys280 is corroborated with a previous mutational study on *E. coli* MiaA, in which its alanine-substituted K280A mutant increased the $K_m$ value for tRNA more than 30 times higher than that of the wild type (32). The second difference in the anticodon stem of $tRNA^{Ser}_{GGA}$ from the $i^6A$ acceptors is the $C_{31}$–$G_{39}$ base pair at the end of the stem. The exocyclic oxygens of the corresponding $U_{39}$ in $tRNA^{Phe}_{GAA}$ make double hydrogen bonds with side chains of Arg167 and Arg281, respectively. However, $U_{39}$ can be replaced by pseudouridine and adenosine in the native isoacceptors, raising a vague necessity for discrimination of this base. The strict conservation of A–U (Ψ) base pair at this position of the isoacceptors (Fig. S2A) suggests that the energy barrier for disruption of the conformation of the anticodon loop with the capping G–C base pair in $tRNA^{Ser}_{GGA}$ is too high for MiaA to modify this particular tRNA, as its substitution by the G–C base pair resulted in increase of the $K_m$ value about three times compared to the wild type (33).

The other notable base-specific interaction is formed between the universally conserved $U_{33}$ and Ser120 in the linker loop. This interaction coordinates the flipped-out $U_{33}$, and likely energetically stabilizes its unfavorable conformation. $U_{33}$ in $tRNA^{Cys}$ complexed with yeast MiaA orthologue forms two hydrogen-bonds with Gln193, corresponding to Gln187 of *E. coli* MiaA (36) (Figs. S1 and S6B). Since Ser120 is variable among MiaA orthologues, it is likely that recognition of $U_{33}$ had diverged among species. In order to stabilize the global conformation of the constrained anticodon loop of the bound tRNA, MiaA possesses large positively-charged patches at the surfaces of both domains that face the approaching tRNA (Fig. 1B). Electrostatic compensation between the backbone phosphate groups of tRNA and

clusters of basic residues, particularly in the invading α14 of the catalytic domain (*ex*. Arg276 and Arg281), and α5 and α8 in the swinging domain (*ex*. Arg130 and Arg167), locks the tRNA in its distorted conformation as a prerequisite for the $A_{37}$ isopentenylation. Besides the electrostatic interactions, the anticodon loop of tRNA is further secured by the base stacking interactions occurred within the tRNA itself and with the protein residues. The helical anticodon stem is extended by coaxial stacking $U_{32}$ with $A_{31}$, and by a triple-base stack composed of $A_{36}$–$A_{38}$–$U_{39}$ (Fig. 2A). The anticodon helix is eventually end-capped by the Trp285 indole ring and the Leu110 side chain, two strictly conserved residues among MiaA orthologues (Fig. S1).

## Dynamic motion of the swinging domain of MiaA

The loss of the electron density map of the swinging domain in the previously published structure indicated that this region of the enzyme is highly flexible in the absence of the bound tRNA (34). However, we further succeeded in carrying out structural determination of the intact apo MiaAs from *Staphylococus epidermidis* and *Bacillus halodurans*, in both of which the swinging domain is entirely visible (Fig. 3B). As predicted, these structures reveal a high freedom of motion of the swinging domain as a consequence of being connected to the catalytic domain via two elongated linker loops. Whereas helical bundles in the swinging domain show rigid and preserved topology, their orientations as well as relative positions to the catalytic domain are extremely varied. The swinging domain of *S. epidermidis* MiaA rotates 70° degrees relative to that of the *E. coli* in complex with the tRNA. By comparison, the *B. halodurans* swinging domain turns away from the catalytic domain by 60° degrees, while extending its linker loop to 30 Å in length with respect to that of the *E. coli*. Consequently, whereas *S. epidermidis* MiaA forms a monomer, that of *B. halodurans* MiaA forms a dimeric structure in their respective crystallographic asymmetric units. This difference likely contributes to stabilization of the swinging domain by two entirely different manners. Every two molecules of *B. halodurans* MiaA unexpectedly makes up the dimer by swapping the swinging domain of each interacting protomer. Surprisingly, this domain-swapping somewhat resembles the MiaA–tRNA complex, as the helix-turn-helix moiety of one swinging domain interacts with the catalytic domain of the interacting protomer, thereby mimicking the anticodon helix of the bound tRNA substrate (Fig. S5A). This suggests a plausible state of intramolecular autoinhibition, at least, in *B. halodurans* MiaA. Moreover, the first helical hairpin (α5 and α6) of the swinging domain forms a wedge topology mimicking the '<' shape of the anticodon loop of bound tRNA, whereby the main chain carboxyl groups play a role in electrostatic interactions similar to the RNA phosphate groups. Taken together, our MiaA structures render the first view of dynamic motion of the swinging domain before and after tRNA binding.

## Sequential binding of the cofactor to MiaA–tRNA complex

To unravel the underlying mechanism of the catalysis, we performed a soaking experiment on the crystal of *E. coli* MiaA–tRNA complex with a nonhydrolyzable DMAPP analog, DMASPP, and determined the ternary structure to a resolution of 2.75 Å. The unbiased *2Fo-Fc* and *Fo-Fc* difference maps clearly indicate that DMASPP ligand is trapped in the middle of the reaction tunnel, where the dimethylallyl group points toward the $A_{37}$ purine ring (Fig. 4). A density peak corresponding to a $Mg^{2+}$ ion is also observed in coordination to the side chain of the invariant Thr24 and the pyrophosphate group of DMASPP. While the pyrophosphate moiety is tightly held via a network of hydrogen bonding with the backbone nitrogen atoms of Ala20-Thr24, the constitutive residues of the conserved P-loop at the N terminus of MiaA, it makes additional charge-charge interactions with the conserved Lys23 (Figs. 4 and S4). The sulfur atom of DMAPP, which mimics the bridging oxygen of DMAPP, forms hydrogen bonds with invariant Thr19 and Arg217 side chains. The environment of the DMAPP-binding site is highly homologous to that of *Agrobacterium tumefaciens* Tzs, a MiaA orthologue, which produces $i^6A$ using AMP instead of tRNA (35). We conclude that the mechanism of

isopentenyltransferase for both RNA and adenine nucleotides are identical in which an invariant Asp42 acts as a general base to abstract a proton from N6 of $A_{37}$ (Figs. 4 and S4). More importantly, while the dimethylallyl group is embedded in the hydrophobic pocket constructed by the terminal methyl moieties of Thr19 and Thr275, and side chains of Met221, Val249, and Leu278, it is stacked with $A_{37}$ of the tRNA. A distance of 3.50 Å between C1 of DMASPP and N6 of $A_{37}$ provides a good distance suitable for the nucleophilic attack. Such a face-to-face stacking between a flipped-out base and a cofactor was first documented in the crystal structure of an rRNA methyltransferase RumA complexed with a fragment of RNA ligand (49). The elimination of the stacking interaction using a riboabasic modification increased the $K_m$ value of the cofactor, thereby attributing an important role of stacking interaction in both cofactor binding and efficient catalysis (49). The stacking between $A_{37}$ and the dimethylallyl group in MiaA, therefore, provides a reasonable explanation for ordered substrate binding by MiaA as previously reported (14).

An alternative interpretation accounting for sequential substrate binding comes from cautious interspecies comparison of our MiaA structures. This approach is feasible as all of our MiaA structures were derived from closely related bacterial species whose MiaA enzymes have high sequence identity with each other (Fig. S1). When focusing on the catalytic domain among our MiaA structures, no global structural change was apparent. The Cα rms deviations among the catalytic domains are kept in a range of 1.08-1.13 Å. However, there is a subtle local conformational change only in the P-loop of *S. epidermidis* MiaA that represents an authentic apo enzyme without any bound substrates, cofactors, and divalent metal ions (Fig. S5B). The P-loop is shifted downward in a manner to constrict the tunnel by approximately 2 Å, where the P-loop makes severe clashes at several points with DMAPP in the overlaid structure of *S. epidermidis* and *E .coli* MiaAs. By comparison, the P loop is open in the MiaA–tRNA complex as well as in the autoinhibited *B. halodurans* MiaA, ready for the cofactor to come into the tunnel, implying that the binding of the tRNA induces a local conformational alteration of the P-loop, allowing the cofactor to be bound.

## Structural comparisons

Comparison of the MiaA structures and its structural homologues reveals that MiaA and small molecule kinases such as guanylate kinases (1GKY; Cα rmsd of 3.2 Å for overall) share same ancestry, despite their amino acid sequences show very low similarity. In MiaA orthologues, the P-loop of kinases has evolved to function as a structural element that recognizes DMAPP instead of ATP, in which the unique Thr19 of MiaA plays an essential role in reaction catalysis, and possibly in gating the cofactor inside the tunnel. Structural comparison of MiaAs and nucleotide kinases, including cytokinin-relevant isopentenyltransferases that produces $i^6A$ exclusively from AMP, ADP or ATP, indicates two structural features which were added to MiaA during evolution so as to ensure the substrate specificity toward tRNA. Specifically, MiaA altered the electrostatic surface property of one side in the catalytic domain to accommodate the RNA backbone, and at the same time, acquired an idiosyncratic helical swinging domain to trap, deform, and discriminate tRNA substrates.

To date, there are five enzymes that modify the anticodon helix of tRNA, whose structures have been solved with their respective intact or fragmentary tRNA substrates that are as follows: *Zymomonas mobilis* tRNA guanine transglycosylase complexed with $ASL^{Tyr}$ (PDB code: *1Q2R*) (50); *Staphylococcus aureus* TadA with $ASL^{Arg}$ (*2B3J*) (51); *E. coli* MnmA with $tRNA^{Glu}$ (*2DEU*) (52); *E. coli* RluA–$ASL^{Phe}$ (*2I82*) (53); and *E. coli* TruA–$tRNA^{Leu}$ (*2NQP*) (54). MiaA–tRNA is the sixth complex, in which the enzyme modifies the nucleotide at position 37. The structures of eukaryotic MiaA orthologue from *Saccharomyces cerevisiae* in complex with $tRNA^{Cys}_{GCA}$ were also recently determined at a resolution range of 2.95-3.6 Å (36). Comparative analysis between the bacterial and eukaryotic Mia–tRNA

complexes emphasizes fundamental mechanism of the two pinching fingers that are conserved in both structures (Arg170-171 in *S. cerevisiae* MiaA). The most substantial difference in tRNA recognition is seen at the first and the second letter of the anticodon, where their phosphate backbones are further deviated by ~4 Å (Fig. S6). An Arg130 in the swinging domain coordinates the phosphate of $A_{35}$ in *E. coli* $tRNA^{Phe}$, whereas the corresponding phosphate of $C_{35}$ in yeast $tRNA^{Cys}$ remains free. These suggest that MiaA possesses a capacity of accommodation for various anticodon sequences that share their 3′-termini by $A_{36}$.

The overlaid structures of all aforementioned ASL structures, including the NMR structure of unmodified $ASL^{Phe}$, and an unconstrained canonical tRNA anticodon, reveal that the anticodon loops exhibit a great magnitude of flexibility by a movement greater than 20 Å. However, these structural rearrangements are utterly distinct in that the exposure of the to-be-modified base into the active site is finely tuned by each corresponding enzyme for proper modification and optimal rate of catalysis. Fascinatingly, these structural alignments also reveal that the anticodon structure in the MiaA–tRNA complex resembles the solution structure of unmodified $ASL^{Phe}$ more than that of the crystal structure of native $tRNA^{Phe}$. It apparently reveals an intermediate state between the conformations of the fully modified and unmodified anticodon loops (Fig. 3A). Our observation corroborates a previous NMR study that suggested an essential role of $i^6A$ in promotion of the canonical U-turn motif, which takes advantage of the favorable base stacking energy. Moreover, the NMR structure of the unmodified $ASL^{Phe}$ possesses an expanded major groove that readily allows the ‘pinching fingers’ to act on it like a ‘press’. Our interpretation naturally leads us to a hypothesis that MiaA is an ‘tRNA chaperone’ that refolds the tRNA anticodon by a ‘pinch-and-flip’ mechanism so as to modify tRNA by an isopentenyl group which in turn, fix the preferable loop conformation before its recruitment to the mRNA decoding on the ribosome (Fig. 5).

In summary, this study has elucidated an exquisite mechanism in isopentenylation of tRNA anticodon containing a consensus $A_{36}A_{37}A_{38}$ sequence for the precise decoding of codons starting with uridine on the basis of the ‘pinch-and-flip’ mechanism of MiaA. A unique helical swinging domain was appended to MiaA during evolution to achieve the RNA ‘refolding’ that leads to creating a canonical anticodon loop structure as a prerequisite for the decoding function of tRNA inside the ribosome. Our results confer animated motions of dynamics derived from both tRNA and enzyme in a process of RNA modification.

## Supplementary Material

Refer to Web version on PubMed Central for supplementary material.

## References

1. Agris PF, Vendeix FA, Graham WD. tRNA’s wobble decoding of the genome: 40 years of modification. Journal of molecular biology 2007;366:1–13. [PubMed: 17187822]
2. Urbonavicius J, Qian Q, Durand JM, Hagervall TG, Bjork GR. Improvement of reading frame maintenance is a common function for several tRNA modifications. EMBO J 2001;20:4863–4873. [PubMed: 11532950]
3. Suzuki, T. Fine-tuning of RNA functions by modification and editing. Vol. 12. Springer-Verlag; NY: 2005. Biosynthesis and function of tRNA wobble modifications.
4. Czerwoniec A, Dunin-Horkawicz S, Purta E, Kaminska KH, Kasprzak JM, Bujnicki JM, Grosjean H, Rother K. MODOMICS: a database of RNA modification pathways. Nucleic Acids Res. 20082008 update
5. Cabello-Villegas J, Tworowska I, Nikonowicz EP. Metal ion stabilization of the U-turn of the A37 N6-dimethylallyl-modified anticodon stem-loop of Escherichia coli tRNAPhe. Biochemistry 2004;43:55–66. [PubMed: 14705931]

6. Cabello-Villegas J, Winkler ME, Nikonowicz EP. Solution conformations of unmodified and A(37)N (6)-dimethylallyl modified anticodon stem-loops of Escherichia coli tRNA(Phe). Journal of molecular biology 2002;319:1015–1034. [PubMed: 12079344]
7. Murphy, FVt; Ramakrishnan, V.; Malkiewicz, A.; Agris, PF. The role of modifications in codon discrimination by tRNA(Lys)UUU. Nat Struct Mol Biol 2004;11:1186–1191. [PubMed: 15558052]
8. Yarian C, Townsend H, Czestkowski W, Sochacka E, Malkiewicz AJ, Guenther R, Miskiewicz A, Agris PF. Accurate translation of the genetic code depends on tRNA modified nucleosides. J Biol Chem 2002;277:16391–16395. [PubMed: 11861649]
9. Kersten H. On the biological significance of modified nucleosides in tRNA. Prog Nucleic Acid Res Mol Biol 1984;31:59–114. [PubMed: 6397775]
10. Sprinzl M, Horn C, Brown M, Ioudovitch A, Steinberg S. Compilation of tRNA sequences and sequences of tRNA genes. Nucleic Acids Res 1998;26:148–153. [PubMed: 9399820]
11. Bartz JK, Kline LK, Soll D. N6-(Delta 2-isopentenyl)adenosine: biosynthesis in vitro in transfer RNA by an enzyme purified from Escherichia coli. Biochem Biophys Res Commun 1970;40:1481–1487. [PubMed: 4326583]
12. Rosenbaum N, Gefter ML. Delta 2 -isopentenylpyrophosphate: transfer ribonucleic acid 2 -isopentenyltransferase from Escherichia coli. Purification and properties of the enzyme. J Biol Chem 1972;247:5675–5680. [PubMed: 4341485]
13. Caillet J, Droogmans L. Molecular cloning of the Escherichia coli miaA gene involved in the formation of delta 2-isopentenyl adenosine in tRNA. J Bacteriol 1988;170:4147–4152. [PubMed: 3045085]
14. Moore JA, Poulter CD. Escherichia coli dimethylallyl diphosphate:tRNA dimethylallyltransferase: a binding mechanism for recombinant enzyme. Biochemistry 1997;36:604–614. [PubMed: 9012675]
15. Leung HC, Chen Y, Winkler ME. Regulation of substrate recognition by the MiaA tRNA prenyltransferase modification enzyme of Escherichia coli K-12. J Biol Chem 1997;272:13073–13083. [PubMed: 9148919]
16. Esberg B, Bjork GR. The methylthio group (ms2) of N6-(4-hydroxyisopentenyl)-2-methylthioadenosine (ms2io6A) present next to the anticodon contributes to the decoding efficiency of the tRNA. J Bacteriol 1995;177:1967–1975. [PubMed: 7536729]
17. Pierrel F, Douki T, Fontecave M, Atta M. MiaB protein is a bifunctional radical-S-adenosylmethionine enzyme involved in thiolation and methylation of tRNA. J Biol Chem 2004;279:47555–47563. [PubMed: 15339930]
18. Diaz I, Pedersen S, Kurland CG. Effects of miaA on translation and growth rates. Mol Gen Genet 1987;208:373–376. [PubMed: 3312947]
19. Hagervall TG, Ericson JU, Esberg KB, Li JN, Bjork GR. Role of tRNA modification in translational fidelity. Biochim Biophys Acta 1990;1050:263–266. [PubMed: 2207153]
20. Bouadloun F, Srichaiyo T, Isaksson LA, Bjork GR. Influence of modification next to the anticodon in tRNA on codon context sensitivity of translational suppression and accuracy. J Bacteriol 1986;166:1022–1027. [PubMed: 3086285]
21. Harrington KM, Nazarenko IA, Dix DB, Thompson RC, Uhlenbeck OC. In vitro analysis of translational rate and accuracy with an unmodified tRNA. Biochemistry 1993;32:7617–7622. [PubMed: 7688564]
22. Petrullo LA, Gallagher PJ, Elseviers D. The role of 2-methylthio-N6-isopentenyladenosine in readthrough and suppression of nonsense codons in Escherichia coli. Mol Gen Genet 1983;190:289–294. [PubMed: 6410151]
23. Connolly DM, Winkler ME. Genetic and physiological relationships among the miaA gene, 2-methylthio-N6-(delta 2-isopentenyl)-adenosine tRNA modification, and spontaneous mutagenesis in Escherichia coli K-12. J Bacteriol 1989;171:3233–3246. [PubMed: 2656644]
24. Blum PH. Reduced leu operon expression in a miaA mutant of Salmonella typhimurium. J Bacteriol 1988;170:5125–5133. [PubMed: 3141379]
25. Buck M, Griffiths E. Iron mediated methylthiolation of tRNA as a regulator of operon expression in Escherichia coli. Nucleic Acids Res 1982;10:2609–2624. [PubMed: 7043398]
26. Buck M, Griffiths E. Regulation of aromatic amino acid transport by tRNA: role of 2-methylthio-N6-(delta2-isopentenyl)-adenosine. Nucleic Acids Res 1981;9:401–414. [PubMed: 7010315]

27. Connolly DM, Winkler ME. Structure of Escherichia coli K-12 miaA and characterization of the mutator phenotype caused by miaA insertion mutations. J Bacteriol 1991;173:1711–1721. [PubMed: 1999389]

28. Miyawaki K, Tarkowski P, Matsumoto-Kitano M, Kato T, Sato S, Tarkowska D, Tabata S, Sandberg G, Kakimoto T. Roles of Arabidopsis ATP/ADP isopentenyltransferases and tRNA isopentenyltransferases in cytokinin biosynthesis. Proc Natl AcadSci USA 2006;103:16598–16603.

29. Spinola M, Galvan A, Pignatiello C, Conti B, Pastorino U, Nicander B, Paroni R, Dragani TA. Identification and functional characterization of the candidate tumor suppressor gene TRIT1 in human lung cancer. Oncogene 2005;24:5502–5509. [PubMed: 15870694]

30. Laezza C, Notarnicola M, Caruso MG, Messa C, Macchia M, Bertini S, Minutolo F, Portella G, Fiorentino L, Stingo S, Bifulco M. N6-isopentenyladenosine arrests tumor cell proliferation by inhibiting farnesyl diphosphate synthase and protein prenylation. FASEB J 2006;20:412–418. [PubMed: 16507758]

31. Motorin Y, Bec G, Tewari R, Grosjean H. Transfer RNA recognition by the Escherichia coli delta2-isopentenyl-pyrophosphate:tRNA delta2-isopentenyl transferase: dependence on the anticodon arm structure. RNA 1997;3:721–733. [PubMed: 9214656]

32. Soderberg T, Poulter CD. Escherichia coli dimethylallyl diphosphate:tRNA dimethylallyltransferase: site-directed mutagenesis of highly conserved residues. Biochemistry 2001;40:1734–1740. [PubMed: 11327834]

33. Soderberg T, Poulter CD. Escherichia coli dimethylallyl diphosphate:tRNA dimethylallyltransferase: essential elements for recognition of tRNA substrates within the anticodon stem-loop. Biochemistry 2000;39:6546–6553. [PubMed: 10828971]

34. Xie W, Zhou C, Huang RH. Structure of tRNA dimethylallyltransferase: RNA modification through a channel. Journal of molecular biology 2007;367:872–881. [PubMed: 17292915]

35. Sugawara H, Ueda N, Kojima M, Makita N, Yamaya T, Sakakibara H. Structural insight into the reaction mechanism and evolution of cytokinin biosynthesis. Proc Natl AcadSci USA 2008;105:2734–2739.

36. Zhou C, Huang RH. Crystallographic snapshots of eukaryotic dimethylallyltransferase acting on tRNA: insight into tRNA recognition and reaction mechanism. Proc Natl Acad Sci U S A 2008;105:16142–16147. [PubMed: 18852462]

37. Acton TB, Gunsalus KC, Xiao R, Ma LC, Aramini J, Baran MC, Chiang YW, Climent T, Cooper B, Denissova NG, Douglas SM, Everett JK, Ho CK, Macapagal D, Rajan PK, Shastry R, Shih LY, Swapna GV, Wilson M, Wu M, Gerstein M, Inouye M, Hunt JF, Montelione GT. Robotic cloning and Protein Production Platform of the Northeast Structural Genomics Consortium. Methods Enzymol 2005;394:210–243. [PubMed: 15808222]

38. Nakamura A, Yao M, Chimnaronk S, Sakai N, Tanaka I. Ammonia channel couples glutaminase with transamidase reactions in GatCAB. Science 2006;312:1954–1958. [PubMed: 16809541]

39. Sherlin LD, Bullock TL, Nissan TA, Perona JJ, Lariviere FJ, Uhlenbeck OC, Scaringe SA. Chemical and enzymatic synthesis of tRNAs for high-throughput crystallization. RNA 2001;7:1671–1678. [PubMed: 11720294]

40. Otwinowski Z, Minor W. Processing of X-ray Diffraction Data Collected in Oscillation Mode. Methods Enzymol 1997;276:307–326.

41. Schneider TR, Sheldrick GM. Substructure solution with SHELXD. Acta Crystallogr D Biol Crystallogr 2002;58:1772–1779. [PubMed: 12351820]

42. Weeks CM, Blessing RH, Miller R, Mungee R, Potter SA, Rappleye J, Smith GD, Xu H, Furey W. Towards automated protein structure determination: BnP, the SnB-PHASES interface. Z Kristallogr 2002;217:686–693.

43. Terwilliger TC, Berendzen J. Automated MAD and MIR structure solution. Acta Crystallogr D Biol Crystallogr 1999;55:849–861. [PubMed: 10089316]

44. Yao M, Zhou Y, Tanaka I. LAFIRE: software for automating the refinement process of protein-structure analysis. Acta Crystallogr D Biol Crystallogr 2006;62:189–196. [PubMed: 16421450]

45. Brunger AT, Adams PD, Clore GM, DeLano WL, Gros P, Grosse-Kunstleve RW, Jiang JS, Kuszewski J, Nilges M, Pannu NS, Read RJ, Rice LM, Simonson T, Warren GL. Crystallography & NMR

system: A new software suite for macromolecular structure determination. Acta Crystallogr D Biol Crystallogr 1998;54:905–921. [PubMed: 9757107]

46. Emsley P, Cowtan K. Coot: model-building tools for molecular graphics. Acta Crystallogr D Biol Crystallogr 2004;60:2126–2132. [PubMed: 15572765]
47. McRee DE. XtalView/Xfit--A versatile program for manipulating atomic coordinates and electron density. J Struct Biol 1999;125:156–165. [PubMed: 10222271]
48. DeLano, WL. DeLano Scientific; Palo Alto, CA, USA: 2002. The PyMOL Molecular Graphics System. http://www.pymol.org
49. Lee TT, Agarwalla S, Stroud RM. A unique RNA Fold in the RumA-RNA-cofactor ternary complex contributes to substrate selectivity and enzymatic function. Cell 2005;120:599–611. [PubMed: 15766524]
50. Xie W, Liu X, Huang RH. Chemical trapping and crystal structure of a catalytic tRNA guanine transglycosylase covalent intermediate. Nat Struct Biol 2003;10:781–788. [PubMed: 12949492]
51. Losey HC, Ruthenburg AJ, Verdine GL. Crystal structure of Staphylococcus aureus tRNA adenosine deaminase TadA in complex with RNA. Nat Struct Mol Biol 2006;13:153–159. [PubMed: 16415880]
52. Numata T, Ikeuchi Y, Fukai S, Suzuki T, Nureki O. Snapshots of tRNA sulphuration via an adenylated intermediate. Nature 2006;442:419–424. [PubMed: 16871210]
53. Hoang C, Chen J, Vizthum CA, Kandel JM, Hamilton CS, Mueller EG, Ferre-D'Amare AR. Crystal structure of pseudouridine synthase RluA: indirect sequence readout through protein-induced RNA structure. Mol Cell 2006;24:535–545. [PubMed: 17188032]
54. Hur S, Stroud RM. How U38, 39, and 40 of many tRNAs become the targets for pseudouridylation by TruA. Mol Cell 2007;26:189–203. [PubMed: 17466622]

## Abbreviations

| | |
|---|---|
| **tRNA** | transfer RNA |
| **DMAPP** | dimethylallyl pyrophosphate |
| **i$^6$A** | $N^6$-isopentenyladenosine |

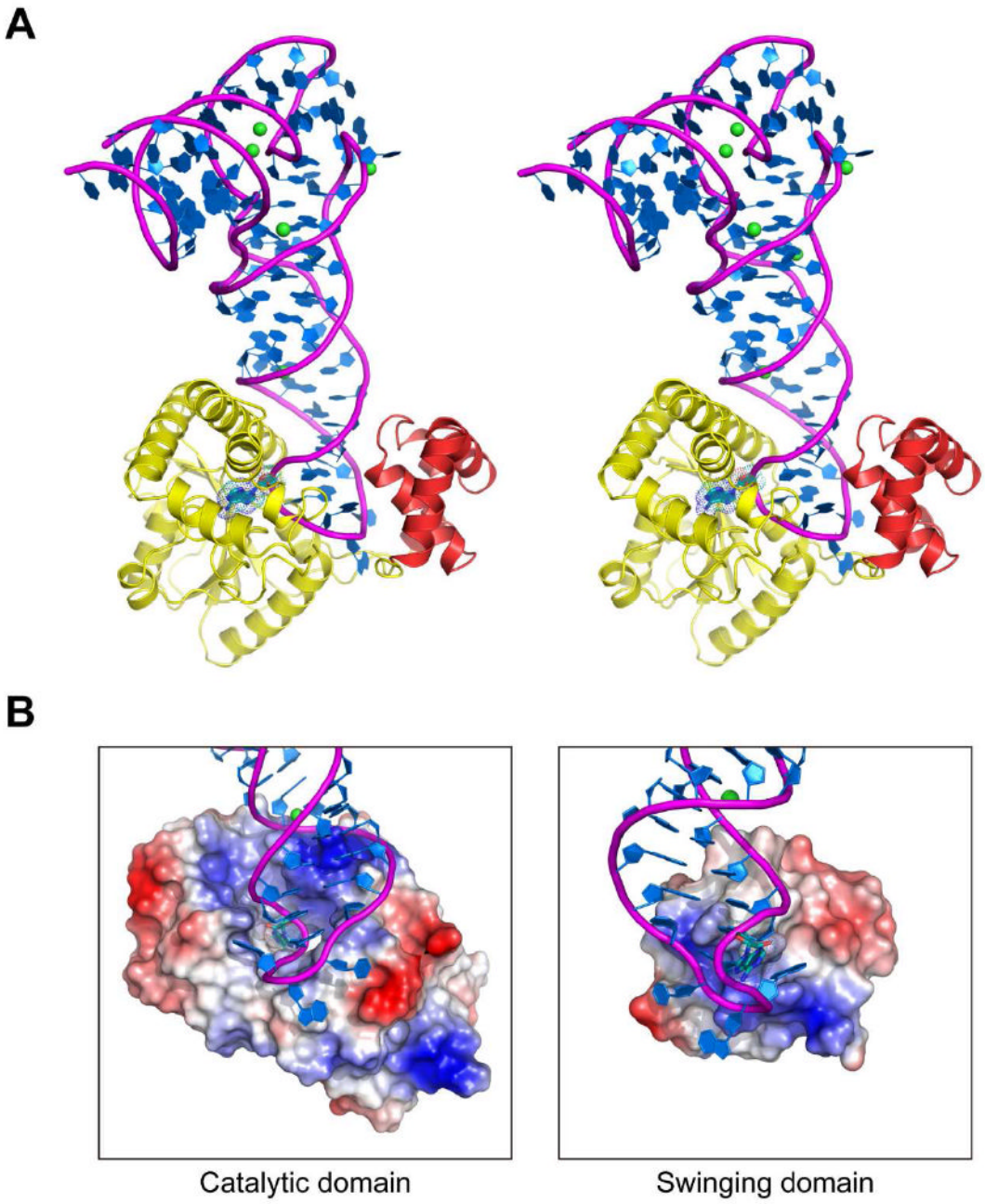


**Figure 1. Overall structure of *E. coli* MiaA–tRNA complex at 2.55 Å**

(**A**) Front-view ribbon representation of the complex in the stereo view, depicted in different colours for each domain: yellow and red for the catalytic domain and the swinging domain, respectively. The bound $tRNA^{Phe}_{GAA}$ is shown in sky blue for its nucleosides, and in magenta for its phosphate backbones. The flipped-out target $A_{37}$ is emphasized by the dotted spheres. $Mg^{2+}$ ion is drawn as green spheres. These colour schemes are used throughout, unless otherwise noted.

(**B**) The shape and the surface charge of the catalytic (left panel) and the swinging domains (right panel) of MiaA in the open-book view of (**A**). The protein solvent-accessible surfaces were generated with the program APBS handled in PyMol(48), and are colored according to their electrostatic potential, from red (-10 *kT/e*) to blue (10 *kT/e*).

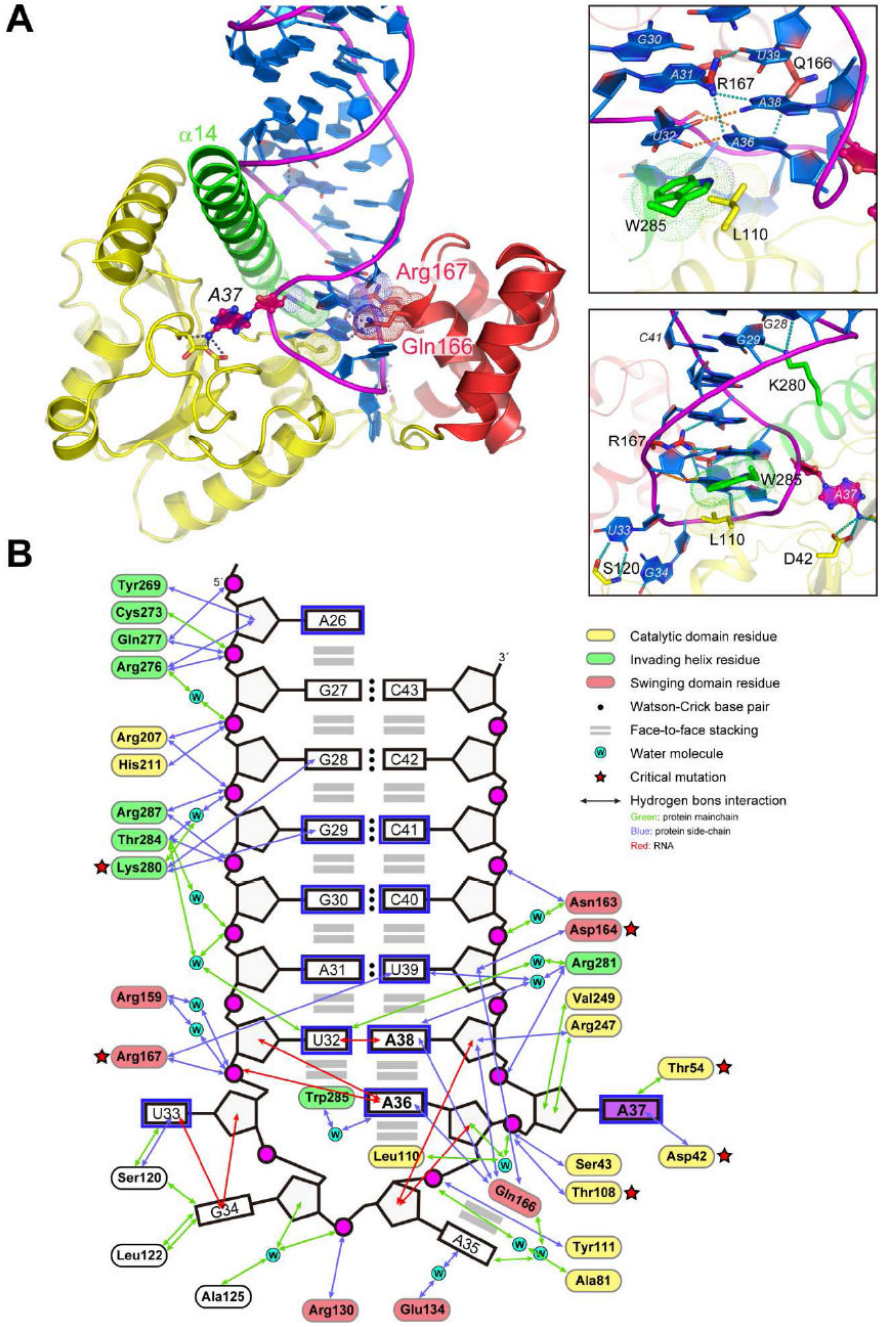


**Figure 2. Interactions between MiaA and tRNA substrate**

(**A**) Remodeling of the tRNA anticodon stem loop by the invading α14 helix (colored in green) and two pinching fingers Gln166 and Arg167 of the swinging domain, which interact with the major and minor grooves, respectively (left panel). The detail of the indirect read out of $A_{36}A_{37}A_{38}$ sequence is shown in the upper right panel, and the direct recognition of tRNA base in the lower. Nucleosides involved in the hydrogen-bonded network with the protein (dashed blue lines) are shown as stick representations and labeled. Interactions between tRNA itself are drawn as red. Two protein residues (Trp285 and Leu110) that end-cap the RNA helix are indicated with dotted spheres.

(**B**) Schematic diagram of tRNA-protein interactions. $A_{37}$ is highlighted with purple, and the backbones of tRNA are shown in pink. Hydrogen bonds have distances less than 3.5 Å. Protein residues that severely affect enzymatic activities are indicated with red stars(32).

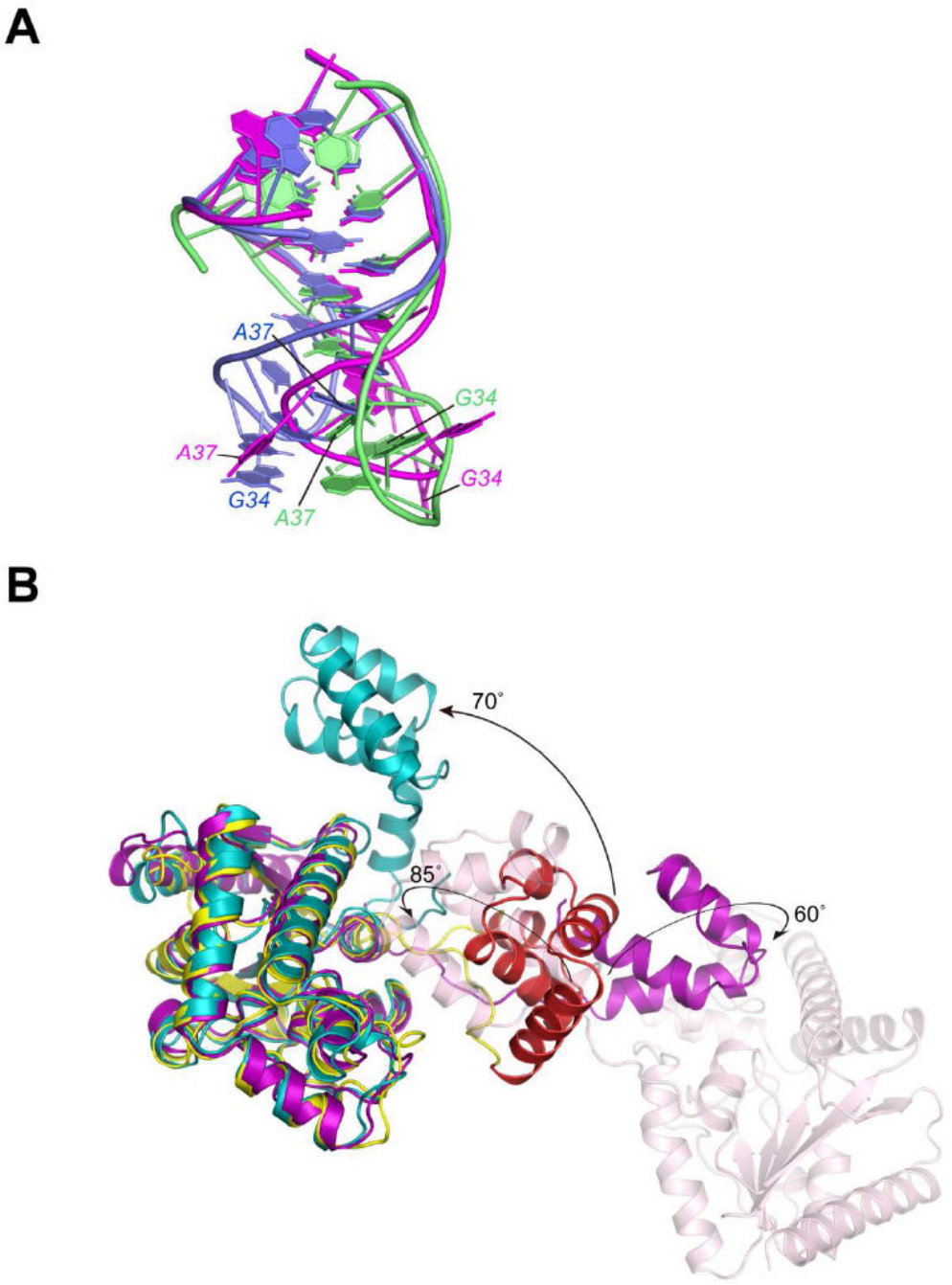


**Figure 3. Dynamics of conformational rearrangement of tRNA and enzyme**

(**A**) Superposition of the tRNA anticodon stem-loop of MiaA-bound *E. coli* $tRNA^{Phe}$ (magenta, a 30° vertically rotated view of Figure 1A) with those of yeast native $tRNA^{Phe}$ (blue, PDB ID code 4TRA) and *E .coli* unmodified NMR structure (green, PDB ID 1KKA)(6). For clarity, the nucleotide sequence of yeast $tRNA^{Phe}$ was manually replaced by that of *E. coli*, and $G_{34}$ and $A_{37}$ are labeled. Only the phosphate atoms of stem nucleotides (27-31 and 39-43) were used for the superposition.

(**B**) $C_\alpha$ superposition of the catalytic domains of *E. coli* MiaA in complex with tRNA, with two apo enzymes from *S. epidermidis* (cyan) and *B. halodurans* (violet). The dimeric counterpart of *B. halodurans* MiaA is also shown in pale pink ribbons. The dynamic structural

changes of the swinging domain of MiaA are indicated with arrows. *E. coli* MiaA is horizontally rotated by 45° compared to Figure 1A.

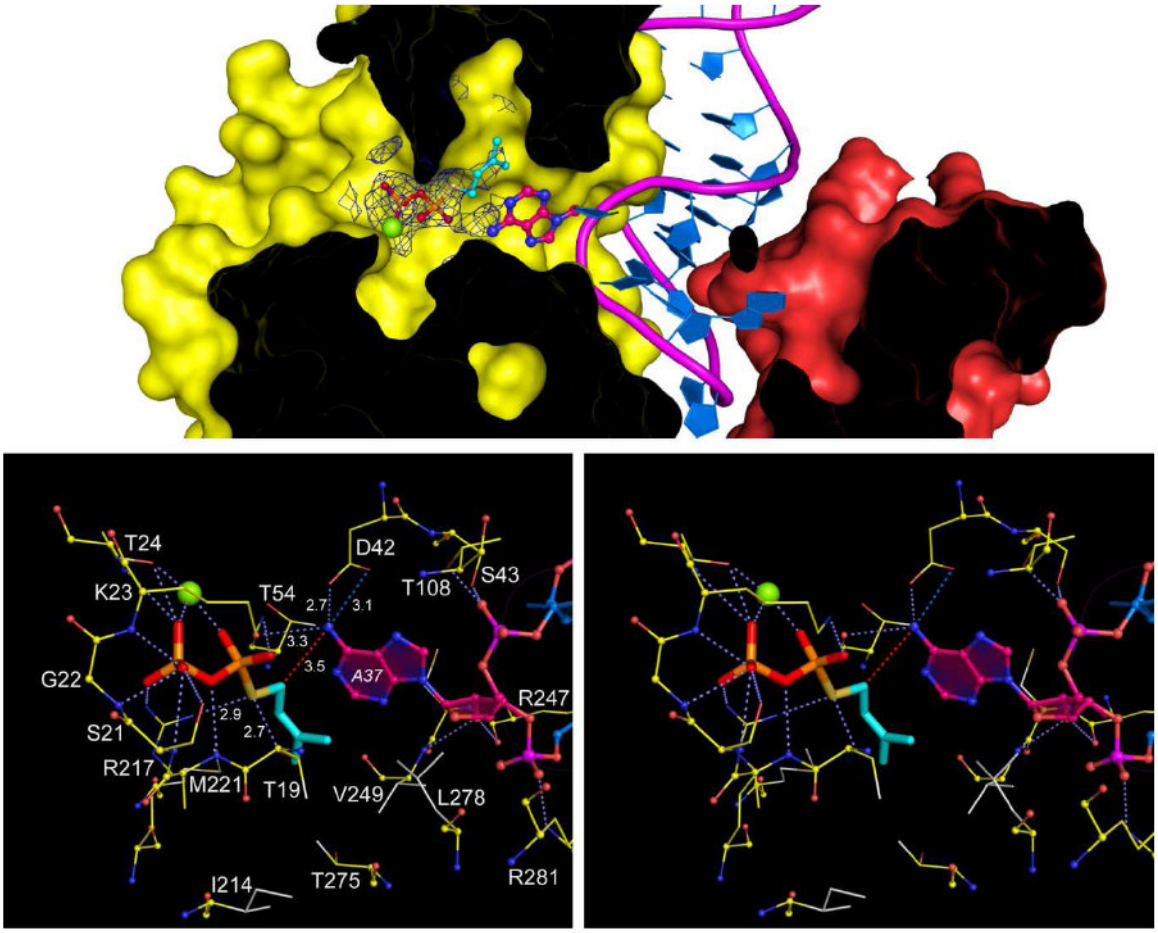


**Figure 4. Mechanism of tRNA isopentenylation in the innermolecular tunnel of MiaA**

Cross-section view of the reaction tunnel in the MiaA–tRNA–DMASPP ternary complex (upper panel). The cofactor analogue DMASPP and a coordinated $Mg^{2+}$ are shown as ball-and-stick representations fitted onto the omit *F*o-*Fc* electron density map (contoured at 1.5$\sigma$, blue mesh) from the soaking crystals. The isopentenyl moiety is colored cyan. The stereo view of the active site illustrating the interactions in recognition of DMASPP and $A_{37}$ is shown in the lower panels with labels for all relevant residues. Protein main chains are depicted as ball-and-stick, and the hydrophobic side chains are highlighted in light gray. The distance of nucleophilic attack between C1 of DMASPP and N6 of $A_{37}$ is indicated with dashed red line, and those between atoms relevant to enzymatic mechanism are also labeled.

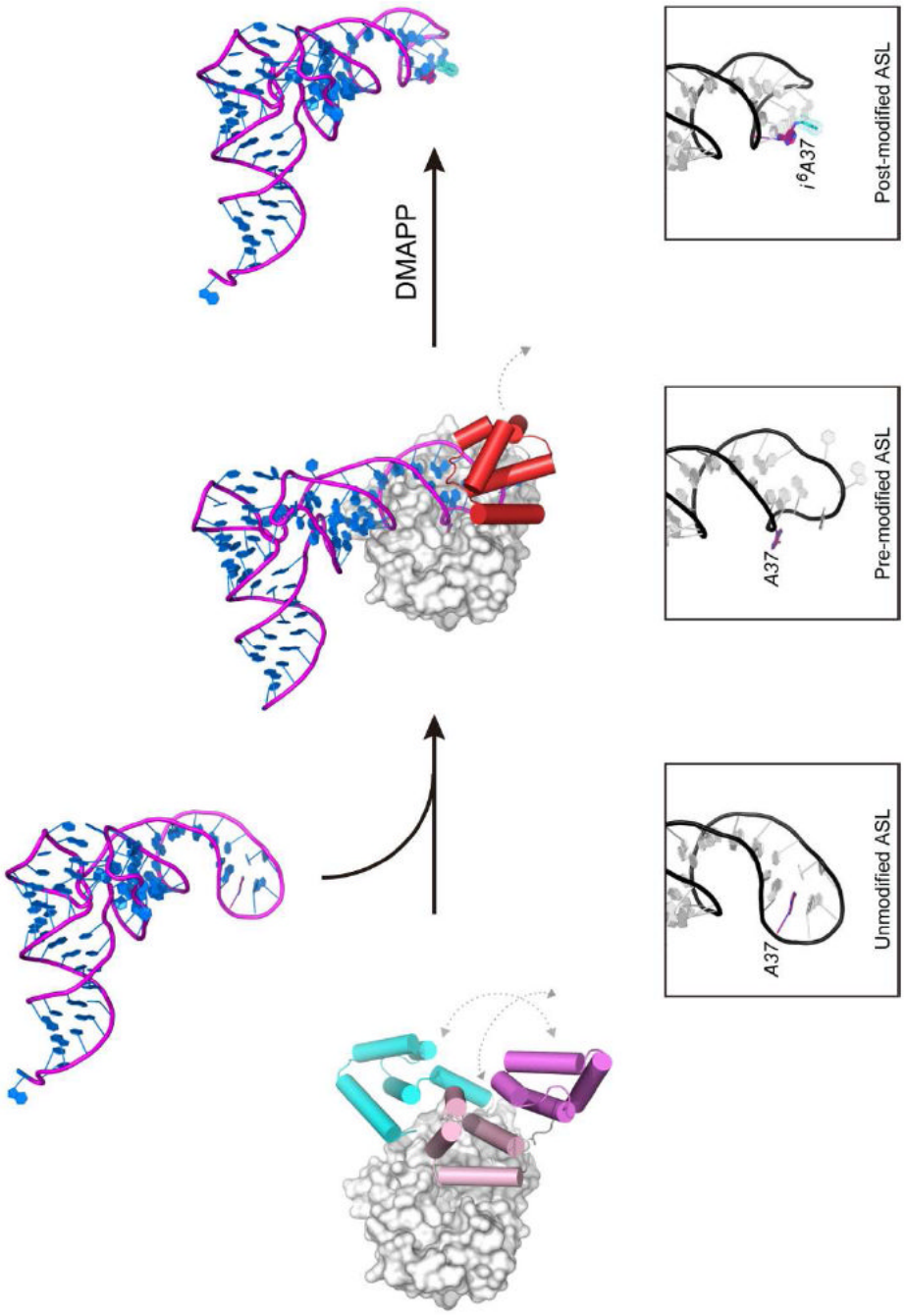


**Figure 5. Proposed model for tRNA chaperone of MiaA**

Shown is the overview of the structural rearrangement along the course of tRNA isopentenylation. The molecular surfaces of the catalytic domain of MiaA are colored light gray, and the swinging domains are drawn by cylindrical helices. The movement of the swinging domain in the crystal structures is indicated by dashed gray arrowed line. The refolding steps of the tRNA anticodon stem-loop during the isopentenyltransferase reaction are summarized in the boxes below.